Zhang et al. Nanoscale Research Letters (2020) 15:163
https://doi.org/10.1186/s11671-020-03397-8

Nanoscale Research Letters

NANO EXPRESS Open Access

The Investigation of Hybrid PEDOT:PSS/β-Ga_2O_3 Deep Ultraviolet Schottky Barrier Photodetectors

Tao Zhang[1,2†], Yixian Shen[1,2†], Qian Feng[1,2*], Xusheng Tian[1,2], Yuncong Cai[1,2], Zhuangzhuang Hu[1,2], Guangshuo Yan[1,2], Zhaoqing Feng[1,2], Yachao Zhang[1,2], Jing Ning[1,2], Yongkuan Xu[3], Xiaozheng Lian[3], Xiaojuan Sun[4], Chunfu Zhang[1,2], Hong Zhou[1,2], Jincheng Zhang[1,2*] and Yue Hao[1,2]

Abstract

In this paper, the hybrid β-Ga_2O_3 Schottky diodes were fabricated with PEDOT:PSS as the anode. The electrical characteristics were investigated when the temperature changes from 298 K to 423 K. The barrier height φ_b increases, and the ideality factor n decreases as the temperature increases, indicating the presence of barrier height inhomogeneity between the polymer and β-Ga_2O_3 interface. The mean barrier height and the standard deviation are 1.57 eV and 0.212 eV, respectively, after taking the Gaussian barrier height distribution model into account. Moreover, a relatively fast response speed of less than 320 ms, high reponsivity of 0.6 A/W, and rejection ratio of $R_{254\ nm}/R_{400\ nm}$ up to 1.26×10^3 are obtained, suggesting that the hybrid PEDOT:PSS/β-Ga_2O_3 Schottky barrier diodes can be used as deep ultraviolet (DUV) optical switches or photodetectors.

Keywords: β-Ga_2O_3, PEDOT:PSS, Hybrid Schottky diodes, Photodetector

Introduction

Many research groups have paid lots of attention to a new ultrawide bandgap semiconductor of β-Ga_2O_3 as a potential material for deep ultraviolet (DUV) photodetectors [1–7], high voltage, and high power devices for its wide band gap (4.8–4.9 eV), high breakdown electric field (8 MV/cm), and chemical stability [8–11]. In addition, it is simple to cleave β-Ga_2O_3 into nanomembranes or thin belts [12, 13] for its unique property of the large lattice constant along [100] direction .Various metals, such as Cu [14], Pd [15], Pt [11, 16–19], Au [15, 20], Ni [16, 21–23], and TiN [18], were used to investigate the electrical characteristics of β-Ga_2O_3 Schottky barrier diodes (SBD). However, the Schottky diodes fabricated with some polymer and the electrical characteristics have not been reported yet. Among all the organic materials, PEDOT:PSS is one of the transparent hole-conducting polymers, whose conductivity is up to 500 S/cm and work function is up to 5.0 ~ 5.3 eV, close to Au and Ni [23–25]. Furthermore, the PEDOT:PSS film can be formed only by spin-coating onto the substrate and subsequent baking in air. There are some investigations in regard to the transparent Schottky contact of PEDOT:PSS on ZnO single crystalline substrate and GaN epilayer, exhibiting rectifying good properties and photoelectrical or photovoltaic characteristics [26–29].

In this work, the hybrid Schottky diode was fabricated with PEDOT:PSS polymer and the mechanically exfoliated β-Ga_2O_3 flakes from the high quality β-Ga_2O_3 substrate. The electrical characteristics of the diodes were investigated in the temperature region between 298 K and 423 K. Furthermore, the I–V measurements under the UV illumination were carried out, the responsivity was measured, and the transient behavior of the photocurrent was also analyzed.

* Correspondence: qfeng@mail.xidian.edu.cn; jchzhang@xidian.edu.cn
†Tao Zhang and Yixian Shen contributed equally to this work.
[1]State Key Discipline Laboratory of Wide Band Gap Semiconductor Technology, School of Microelectronics, Xidian University, Xi'an 710071, China
Full list of author information is available at the end of the article

© The Author(s). 2020 **Open Access** This article is licensed under a Creative Commons Attribution 4.0 International License, which permits use, sharing, adaptation, distribution and reproduction in any medium or format, as long as you give appropriate credit to the original author(s) and the source, provide a link to the Creative Commons licence, and indicate if changes were made. The images or other third party material in this article are included in the article's Creative Commons licence, unless indicated otherwise in a credit line to the material. If material is not included in the article's Creative Commons licence and your intended use is not permitted by statutory regulation or exceeds the permitted use, you will need to obtain permission directly from the copyright holder. To view a copy of this licence, visit http://creativecommons.org/licenses/by/4.0/.

Experimental Methods

The β-Ga_2O_3 flakes with the thicknesses of 15–25 μm were mechanically exfoliated from the (100) β-Ga_2O_3 substrate with the electron concentration of 7 × 10^{16} cm^{-3}. For the electron density is 2–3 orders of magnitude higher than that in the unintentionally doped Ga_2O_3 epilayer deposited on sapphire substrate in [30] and the highly conductive PEDOT:PSS films was used in this paper, so the pn heterojunction was formed in [30] while Schottky junction was formed in this paper [30]. Figure 1a shows the schematic diagram of the hybrid PEDOT:PSS/β-Ga_2O_3 Schottky diode. The β-Ga_2O_3 flakes were cleaned in acetone, ethanol, and deionized water with ultrasonic agitation and then immersed into the HF: H_2O (1:10) solution to remove surface oxides. Then, the deposition of Ti/Au(20 nm/100 nm) metal stack was carried out on the whole back side, and the rapid thermal processing at 470 °C under N_2 atmosphere was conducted for 60 s to decrease the ohmic contact resistance. After spin coated onto the surface of β-Ga_2O_3 flake for three times, PEDOT:PSS was baked on an electric hotplate at 150 °C, and the baking duration was 15 min. Subsequently, isolated devices with the area of 1 mm × 2 mm were obtained. From the HRTEM image of Fig. 1b, we can observe that the atoms are regularly arranged and few atomic column misalignments are present, indicating a high crystal quality of the β-Ga_2O_3 flake. As shown in Fig. 1c, d, the FWHM of HRXRD is about 35.3 arcsec, and the root mean square (RMS) is estimated to be 0.19 nm, illustrating the superior crystal quality and smooth surface.

Result and Discussion

I–V Characteristics and Barrier Height

As presented in Fig. 2a, the I–V characteristics of the hybrid PEDOT:PSS/β-Ga_2O_3 Schottky barrier diodes were investigated when the temperature changes from 298 K to 423 K. The current increases monotonously with the temperature and the semi-log I–V curves show the linear behavior as the forward voltage bias less than 1.5 V. As the forward bias voltage further increases, the slope of the semi-log I–V curves gradually reduces, and the forward current approaches 6 ~ 8 × 10^{-4} A, indicating that the series resistance causes the I–V curve deviating from the linearity. In addition, the reverse leakage current is less than 10^{-9} A at − 3 V, and the I_{on}/I_{off} ratio is up to 10^6 at room temperature, illustrating a rectifying behavior as good as inorganic β-Ga_2O_3 Schottky diodes [11–15].

According to the equation $I = I_s\{\exp[\frac{q(V - IR_s)}{nkT}] - 1\}$ where V is the bias voltage, T and k are the absolute temperature and the Boltzmann constant, respectively. The ideality factor n and the reverse saturation current

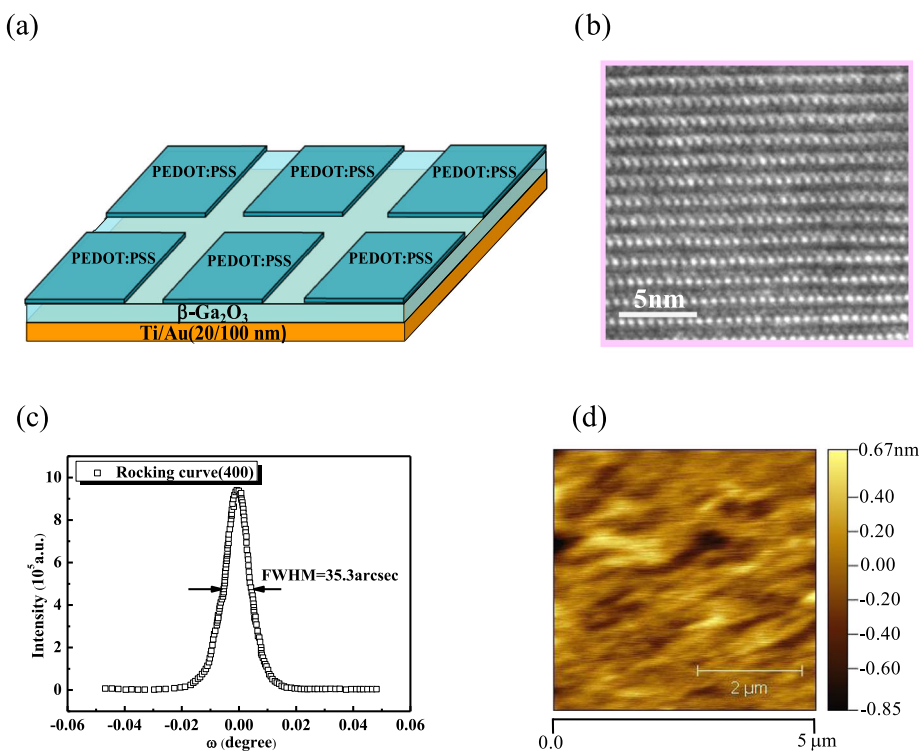

Fig. 1 Schematic diagram of the hybrid PEDOT:PSS/β-Ga_2O_3 Schottky diode (**a**), HRTEM image (**b**), HRXRD rocking curve of the (400) plane (**c**), AFM image of β-Ga_2O_3 flake obtained from β-Ga_2O_3 substrate by mechanically exfoliation, showing a high crystal quality and smooth surface (**d**)

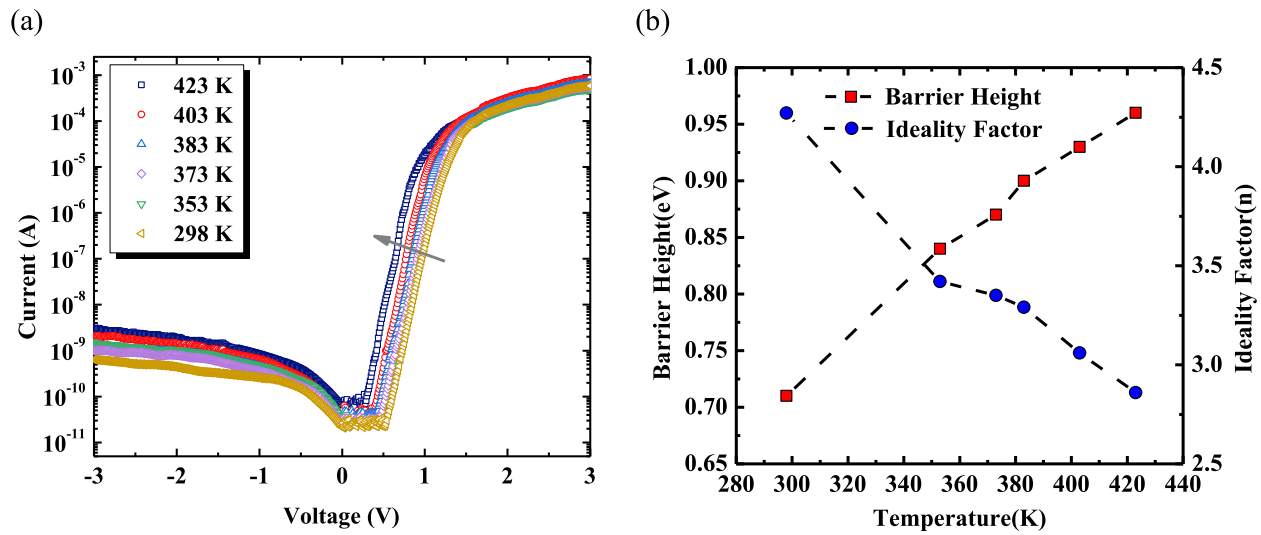

Fig. 2 Temperature-dependent I–V characteristics of PEDOT:PSS/β-Ga_2O_3 SBDs from 298 to 423 K (**a**) and Schottky barrier height φ_b and ideality factor n of hybrid β-Ga_2O_3 SBD (**b**)

I_s can be extracted from the y-axis intercepts and the slopes of the linear extrapolation of the semi-log I–V curves at different temperatures. Although the ideality factor n of the ideal Schottky diode is equal to 1, it is always larger than 1 to some extent in actual device. The deviation of the thermal emission (TE) model becomes much greater as n increases. According to the expression $\phi_b = \frac{kT}{q}\ \ln\left[\frac{AA^*T^2}{I_s}\right]$, we can obtain the Schottky barrier height ϕ_b at different temperatures, as shown in Fig. 2b. The increase in temperature causes ϕ_b to increase from 0.71 eV to 0.84, 0.87, 0.90, 0.93, and 0.96 eV while n to decrease from 4.27 to 3.42, 3.35, 3.29, 3.06, and 2.86. For n much larger than 1, suggesting other conducting mechanisms, such as field effect or thermal field effect, contributing to the current transport and resulting in the difference between pure TE model and the I–V characteristics, which has been illustrated in the wide bandgap SBDs, including GaN and SiC [31–34].

For ϕ_b and n are temperature-dependent, the inhomogeneity of barrier height should be considered at PEDOT:PSS and β-Ga_2O_3 interface. Considering the Gaussian distribution of the barrier height, the inhomogeneous barrier height may be described as $\phi_b = \overline{\phi_{b0}}(T = 0) - \frac{q\sigma_s^2}{2kT}$ and the variation of n with T is given by $(\frac{1}{n} - 1) = \rho_2 - \frac{q\rho_3}{2kT}$, where $\overline{\phi_{b0}}$ and σ_s are the mean barrier height and the standard deviation, respectively, ρ_2 and ρ_3 are the temperature-dependent voltage coefficients, and the voltage deformation of the Schottky barrier height (SBH) distribution was quantified by them (Fig. 3a). $\overline{\phi_{b0}}$ and σ_s can be calculated from the intercept and the slope of the ϕ_b versus $q/2kT$ curve, about 1.57 eV and 0.212 eV, respectively. At the same time, ρ_2 and ρ_3 are evaluated to be 0.4 eV and 0.02 eV from the intercept and slope of the $(1/n - 1)$ versus $q/2kT$ plot. Compared with $\overline{\phi_{b0}}$, σ_s is not small, illustrating the existence of barrier inhomogeneity at PEDOT:PSS/β-Ga_2O_3 interface [35].

By considering the barrier height inhomogeneity, the relationship between the reverse saturation current I_s and the mean barrier height $\overline{\phi_{b0}}$can be modified as $\mathrm{In}(\frac{I_s}{T^2}) - (\frac{q^2\sigma_s^2}{2k^2T^2}) = \mathrm{In}(AA^*) - \frac{q\overline{\phi_{b0}}}{kT}$. It can be discerned from Fig. 3b that the plot of the $\ln(I_s/T^2) - (q^2\sigma_s^2/2k^2T^2)$ versus $1/kT$ is a straight line, from which we can extract the effective Richardson constant A^* of 3.8 A $cm^{-2}K^{-2}$, one order magnitude smaller than the theoretical Richardson constant of 40.8 A $cm^{-2}K^{-2}$ with the β-Ga_2O_3 effective mass of m^* = 0.34 m_0 [36, 37]. Thus, the temperature-dependent ϕ_b and n, in other words, the Gaussian distribution of the barriers over SBHs can be used to explain the barrier inhomogeneity at the PEDOT:PSS/β-Ga_2O_3 interface.

Characteristics of UV Photodetector

As described above, the hybrid β-Ga_2O_3 Schottky diode exhibits a good rectifying characteristics; the ratio of I_{on}/I_{off} up to 10^6 in dark state at room temperature. The lower dark current I_{dark} of 9.4 nA@V_{bias} = − 4 V can be determined from Fig. 4a, indicating a lower noise characteristic. While under the normal incidence of 254 nm wavelength with the photodensity of 150 μW/cm^2, the photocurrent I_{photo} reaches 112 nA@V_{bias} = − 4 V. In addition, the photodetector shows a weak photovoltaic effect with a photocurrent of 0.45 nA at 0 V and an

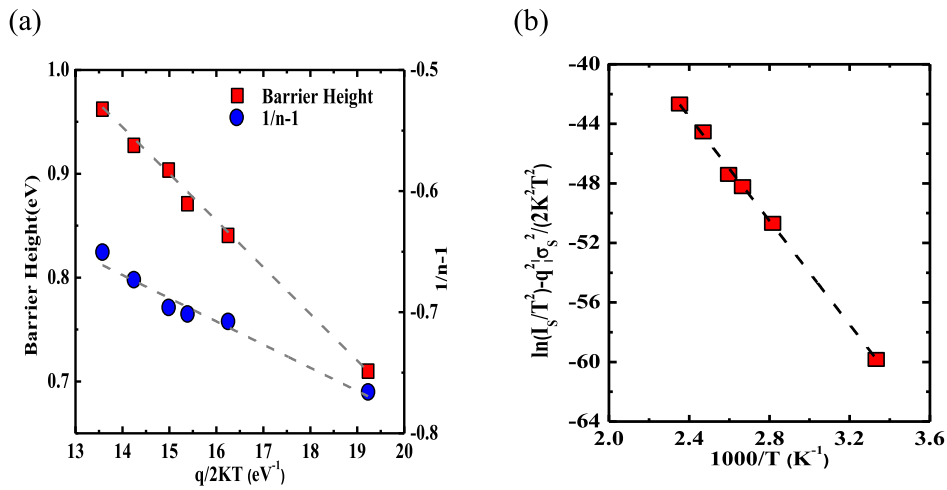

Fig. 3 The variation of the SBH φ_b and (n^{-1} − 1) with $q/2KT$ curves, $\overline{\varphi_{b0}}$ and σ_s can be obtained (**a**), modified $\ln(I_s/T^2) - (q^2\sigma_s^2/2k^2T^2)$ versus 1000/T plot (**b**)

open-circuit voltage (V_{oc}) of 0.15 V, much less than 0.9 V in reference [38], which may be attributed to the carrier density difference and the resulting Fermi level variation. Figure 4b represents the linear I_{photo} versus V_{bias} at various P_{light}. The device shows the dependence of I_{photo} on the P_{light}, and the I_{photo} increases non-linearly with the P_{light}, in other words, at different $V_{bias,}$ the plots of I_{photo} versus P_{light} demonstrate an obvious superlinear behavior, as shown in Fig. 4c. In order to elucidate the mechanism of the superlinear behavior, Fig. 4e presents the energy diagram of the PEDOT:PSS and β-Ga_2O_3 before contact. The electron affinity and the bandgap of β-Ga_2O_3 are 4.0 eV and 4.9 eV, respectively. The lowest unoccupied molecular orbital (LUMO) is 3.3 eV, and the highest occupied molecular orbital of PEDOT:PSS is 5.2 eV [39]. As they came to contact, a Schottky barrier was formed. When the device is illuminated and the reverse bias is applied to the electrodes of the Schottky diodes, the photo generated electron-hole pairs are separated rapidly by the electric field and the holes drift to the anode while the electrons to the cathode, as shown in Fig. 4f. For the presence of traps at the PEDOT: PSS/β-Ga_2O_3 interface, the holes are trapped at the interface states and produce net positive charges, reducing the effective Schottky barrier height, more carriers flowing across the Schottky junction, and improving the I_{photo}. Figure 4d presents the photo to dark current ratio (PDCR) curves under different P_{light}. As the voltage bias shifts from

0V to − 1.2V, the PDCR increases gradually and then decreases with the voltage bias becoming more negative, the higher PDCR above 20 is achieved at a V_{bias} of − 1.2 V and a P_{light} of 150 μW/cm^2.

The time-dependent photoresponse characteristics of hybrid photodetector are studied by using square wave light with a period of 10 s under the V_{bias} of − 1.2 V and a P_{light} of 150 μW/cm^2. After several illumination cycles, devices reach the stable on-state I_{photo} at the given P_{light} and V_{bias}, as represented in Fig. 5a. The rise time and decay time are 319 ms and 270 ms [40, 41], respectively, much less than those of devices fabricated on epitaxial β-Ga_2O_3 films or β-Ga_2O_3 flakes [35, 42, 43] but longer than the data in [31]. For the existence of double heterojunction in [31], PEDOTT:PSS/Ga_2O_3 upper junction and Ga_2O_3/p-Si lower junction, the photogenerated carriers can be separated more effectively by the double built-in electric fields than the only one PEDOTT:PSS/Ga_2O_3 junction in this paper. Therefore, less carriers can be captured by the defects in [31], resulting in the shorter rise time and decay time. Furthermore, the overshooting feature can be observed from the shapes of photoresponse curves with a wedgy head at the lower P_{light} of 150 μW/cm^2 than that occurred at the P_{light} of 600 μW/cm^2 in [30] for the effective collection of photogenerated carriers under the reverse bias of − 1.2 V rather than 0 V.

Figure 6 depicts the responsivity characteristics versus the illumination optical λ under the V_{bias} of − 1.2 V. The maximum responsivity R_{max} of 0.62 A/W is achieved at a λ of 244 nm and the corresponding external quantum efficiency(EQE) of 3.16 × 10^2% calculated by the expression EQE = $hcR_{max}/(e\lambda)$, much higher than that obtained in [30, 38] for the effective collection of photogenerated carriers, where R_{max} is the peak responsivity, and h is the Plank constant. e and λ are the electronic charge and the illumination wavelength, respectively. As the wavelength is longer than 290 nm, the photoresponsivity is lower than 1 × 10^{-3}, illustrating a much better spectral selectivity in the hybrid β-Ga_2O_3 devices. At the same time, the rejection ratio of $R_{254\ nm}/R_{400\ nm}$ is determined

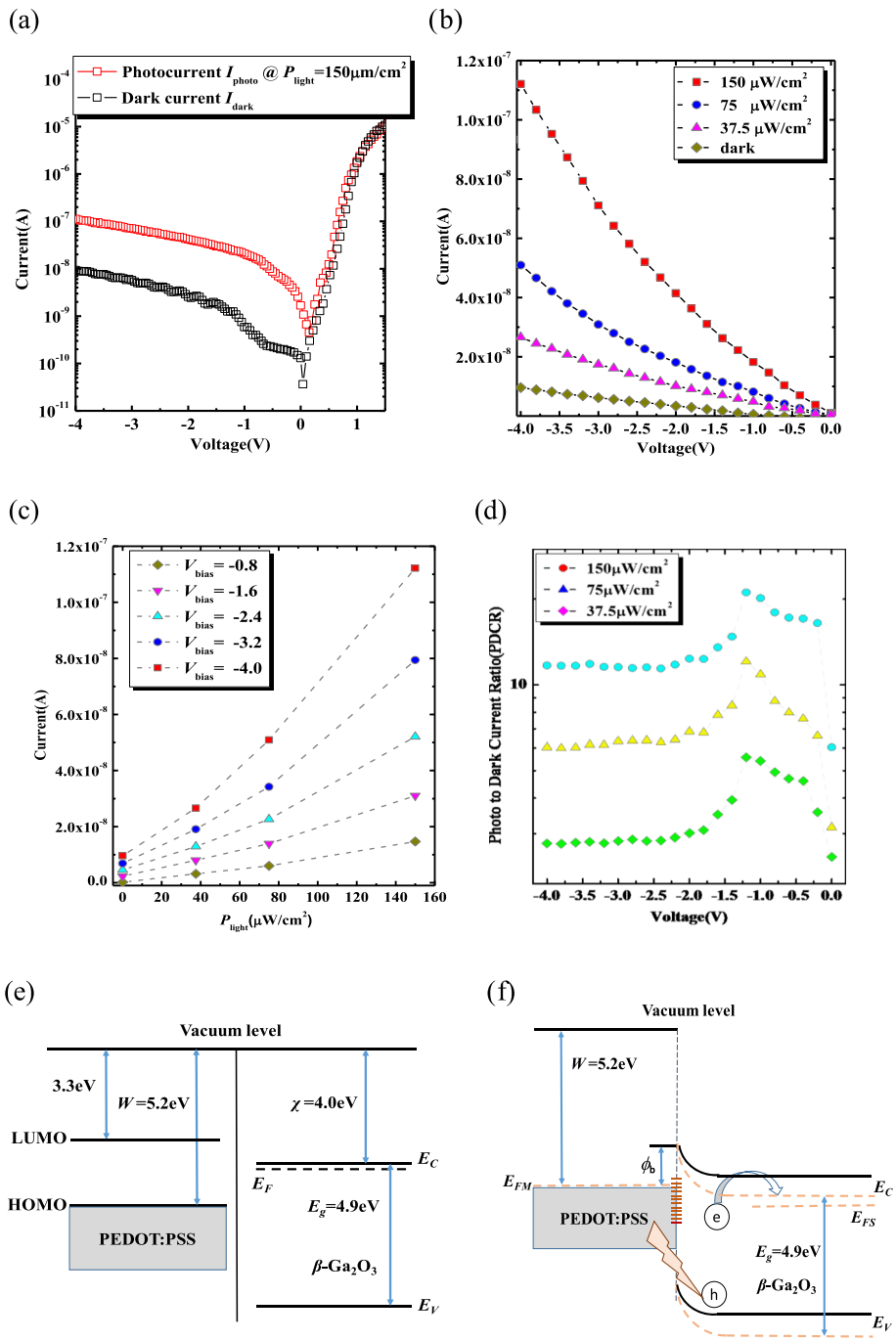

Fig. 4 Relationship between Photocurrent I_{photo}@150 μW/cm^2, dark current I_{dark}, and bias voltage V_{bias} (**a**), plots of I_{photo} versus V_{bias} under different P_{light} (**b**), linear I_{photo} as a function of P_{light} (**c**), curves of photo to dark current ratio (PDCR) under different P_{light} (**d**), band diagram of PEDOT:PSS and β-Ga_2O_3 before contact (**e**), band diagram of PEDOT:PSS and β-Ga_2O_3 under the reverse bias after contact, the condition without applied voltage and the condition with the reverse bias are shown by the solid line and the dashed line, respectively (**f**)

to be 1.26 × 10^3. Compared with the reported inorganic Ga_2O_3 photodetector [43–49], the hybrid device possesses a higher photoresponsivity, faster response speed and larger UV/visible rejection ratio, implying a promising solar blind photodetectors with high performance.

Conclusions

We have fabricated PEDOT:PSS/β-Ga_2O_3 hybrid Schottky barrier diode. The Schottky barrier height ϕ_b and ideality factor n are dependent on temperature, indicating that the Schottky barrier height was inhomogeneous at PEDOT:PSS/β-Ga_2O_3 interface. The mean

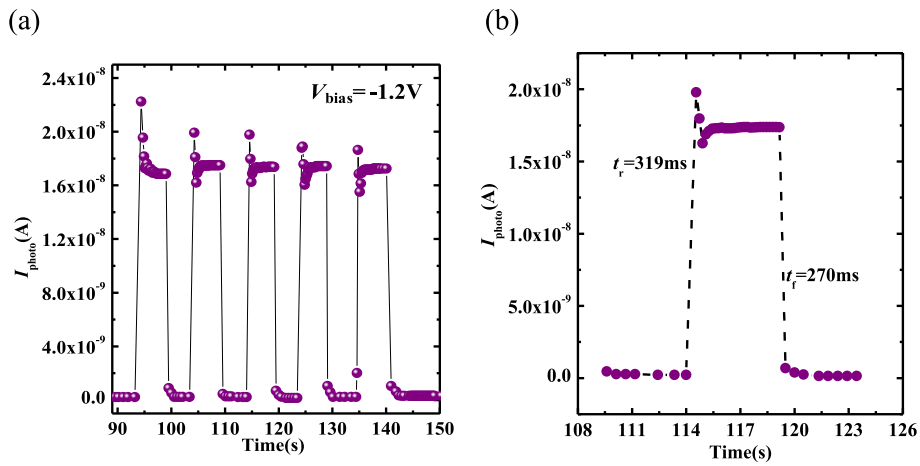

Fig. 5 Multi-cycles (**a**) and single cycle (**b**) of time-dependent I_{photo} of the hybrid PEDOT:PSS/β-Ga_2O_3 Schottky barrier photodetector at the V_{bias} = − 1.2 V, the rise time and decay time are determined to be 319 ms and 270 ms, respectively

barrier height and standard deviation can be evaluated to be 1.57 eV and 0.212 eV, respectively, based on the Gaussian barrier height distribution model. Furthermore, the characteristics of PEDOT:PSS/β-Ga_2O_3 DUV Schottky barrier photodetectors were also investigated. A higher responsivity of 0.6 A/W, rejection ratio of $R_{254\ nm}/R_{400\ nm}$ = 1.26 × 10^3, EQE of 3.16 × 10^4% and a faster response speed of less than 320 ms are achieved, suggesting that the hybrid Schottky barrier diodes can be used as DUV optical switches or photodetectors.

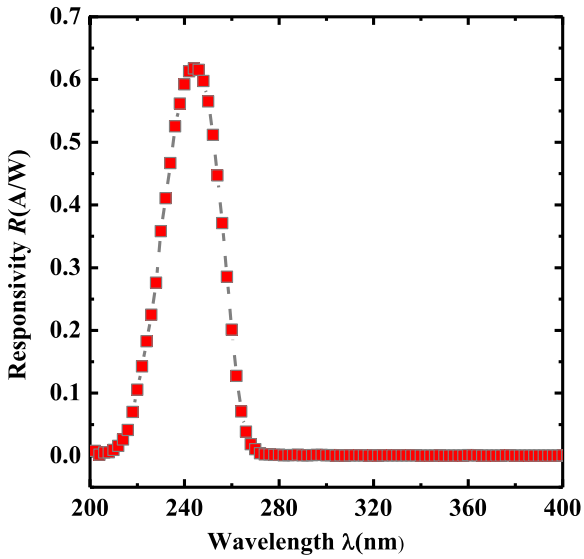

Fig. 6 Responsivity versus wavelengths for the PEDOT:PSS/Ga_2O_3 hybrid photodetectors at V_{bias} =-1.2 V

Abbreviations
AFM: Atomic force microscope; DUV: Deep ultraviolet; EQE: External quantum efficiency; FWHM: Full-width half maximum; HRTEM: High-resolution transmission electron microscopy; LUMO: Lowest unoccupied molecular orbital; PDCR: Photo to dark current ratio; RMS: Root mean square; SBDs: Schottky barrier diodes; TE: Thermal emission

Acknowledgements
Not applicable.

Authors' Contributions
TZ and YS conceived the experiment, performed syntheses, image, and date analysis, and wrote the manuscript. QF, ZH, and ZF gave some important suggestions and instrument. YC performed syntheses, XRD characterization, and AFM image. GY and XT performed electrical testing and optical testing. All authors agree with the document. All authors read and approved the final manuscript.

Funding
In this study, the National Natural Science Foundation of China (Grant Nos. 61774116, 61974112, and 61974115), the 111 Project 2.0 (Grant No. BP2018013), the National key Research and Development Program of China (Grant No. 2018YFB0406500), and State Key Laboratory of Luminiscence and Applications (Grant No. SKLA-2020-04) gave us adequate financial support.

Availability of Data and Materials
All data is available from the authors via a reasonable request.

Competing Interests
The authors declare that they have no competing interests.

Author details
[1]State Key Discipline Laboratory of Wide Band Gap Semiconductor Technology, School of Microelectronics, Xidian University, Xi'an 710071, China. [2]Shaanxi Joint Key Laboratory of Graphene, School of Microelectronics, Xidian University, Xi'an 710071, China. [3]China Electronics Technology Group Corporation No. 46 Research Institute, Tianjin 300220, China. [4]State Key Laboratory of Luminescence and Applications, Changchun Institute of Opeics, Chinese Academy of Sciences, Changchun 130033, China.

Received: 31 October 2019 Accepted: 5 August 2020
Published online: 14 August 2020

References

1. Yu FP, Ou SL, Wuu DS (2015) Pulsed laser deposition of gallium oxide films for high performance solar-blind photodetectors. Opt. Mater. Express 5(5):1240
2. Guo D, Wu Z, Li P, An Y, Liu H, Guo X, Yan H, Wang G, Sun C, Li L, Tang W (2014) Fabrication of β-Ga_2O_3 thin films and solar-blind photodetectors by laser MBE technology. Opt. Mater 4(5):1067
3. Oh S, Jung Y, Mastro MA, Hite JK, Eddy CR, Kim J (2015) Development of solar-blind photodetectors based on Si-implanted β-Ga2O3. Opt. Express 23(22):28300
4. An YH, Zhi YS, Cui W, Zhao XL, Wu ZP, Guo DY, Li PG, Tang WH (2017) Thickness tuning photoelectric properties of β-Ga2O3 thin film based photodetectors. J Nanosci Nanotechnol 17(12):9091–9094
5. Li WH, Zhao XL, Zhi YS, Zhang XH, Chen ZW, Xu XL, Ang HJ, Wu ZP, Tang WH (2018) Fabrication of cerium-doped β-Ga2O3 epitaxial thin films and deep ultraviolet photodetectors. Appl. Optics 57(3):538–543
6. Li S, Guo DY, Li PG, Wang X, Wang YH, Yan ZY, Liu Z, Zhi YS, Huang YQ, Wu ZP, Tang WH (2019) Ultrasensitive,superhigh signal-to-noise ratio,self-powered solar-blind photodtector based on n-Ga2O3/p-CuSCN core-shell microwire heterojunction. ACS Appl.Mater.Interfaces 11(38):35105–35114
7. Zhao XL, Wu ZP, Zhi YS, An YH, Cui W, Li LH, Tang WH (2017) Improvement for the performance of solar-blind photodetector based on β-Ga2O3 thin films by doping Zn. J.Phys.D: Appl. Phys 50(8):085102
8. Higashiwaki M, Sasaki K, Kuramata A, Masui T, Yamakoshi S (2012) Gallium oxide (Ga2O3) metal-semiconductor field-effect transistors on single-crystal β-Ga2O3 (010) substrates. Applied Physics Letters 100(1):013504
9. Armstrong AM, Crawford MH, Jayawardena A, Ahyi A, Dhar S (2016) Role of self-trapped holes in the photoconductive gain of β-gallium oxide Schottky diodes. J Appl Physics 119(10):103102
10. Higashiwaki M, Sasaki K, Murakami H, Kumagai Y, Koukitu A, Kuramata A, Masui T, Yamakoshi S (2016) Recent progress in Ga_2O_3 power devices. Semiconductor Sci Technol 31(3):034001
11. Sasaki K, Higashiwaki M, Kuramata A, Masui T, Yamakoshi S (2013) Ga_2O_3 Schottky barrier diodes fabricated by using single-crystal β-Ga_2O_3(010) substrates. IEEE Electron Device Letters 34:493
12. Zhou H, Si M, Alghamdi S, Qiu G, Yang L, Ye PD (2017) High-performance depletion/enhancement-mode β- Ga_2O_3 on insulator (GOOI) field-effect transistors with record drain currents of 600/450 mA/mm. IEEE Electron Device Lett 38:103–106
13. Hu Z, Zhou H, Dang K, Cai Y, Feng Z, Gao Y, Feng Q, Zhang J, Hao Y (2018) Lateral beta-Ga_2O_3 Schottky barrier diode on sapphire substrate with reverse blocking voltage of 1.7 kV. IEEE J Electron Devices Society 6:815–820
14. Splith D, Müller S, Schmidt F, Von Wenckstern H, van Rensburg JJ, Meyer WE, Grundmann M (2014) Determination of the mean and the homogeneous barrier height of Cu Schottky contacts on heteroepitaxial β-Ga_2O_3 thin films grown by pulsed laser deposition. Phys. Status Solidi A 211(1):40–47
15. Farzana E, Zhang Z, Paul PK, Arehart AR, Ringel SA (2017) Influence of metal choice on (010) β- Ga_2O_3 Schottky diode properties. Appl. Phys. Lett 110(20):202102
16. Ahn S, Ren F, Yuan L, Pearton SJ, Kuramata A (2017) Temperature-dependent characteristics of Ni/Au and Pt/Au Schottky diodes on β- Ga_2O_3. ECS J. Solid State. Sc 6:68–72
17. He Q, Mu W, Dong H, Long S, Jia Z, Lv H, Liu Q, Tang M, Tao X, Liu M (2017) Schottky barrier diode based on β- Ga_2O_3 (100) single crystal substrate and its temperature-dependent electrical characteristics. Appl. Phys. Lett 110(9):093503
18. Tadjer MJ, Wheeler VD, Shahin DI, Eddy CR, Kub FJ (2017) Thermionic emission analysis of TiN and Pt Schottky contacts to β- Ga_2O_3. ECS J. Solid State. Sc 6(4):165–168
19. Higashiwaki M, Konishi K, Sasaki K, Goto K, Nomura K, Thieu QT, Togashi R, Murakami H, Kumagai Y, Monemar B (2016) Temperature-dependent capacitance–voltage and current–voltage characteristics of Pt/Ga_2O_3 (001) Schottky barrier diodes fabricated on n- Ga_2O_3 drift layers grown by halide vapor phase epitaxy. Appl. Phys. Lett 108(13):133503
20. Mohamed M, Irmscher K, Janowitz C, Galazka Z, Manzke R, Fornari R (2012) Schottky barrier height of Au on the transparent semiconducting oxide β-Ga_2O_3. Appl. Phys. Lett 101(13):132106
21. Irmscher K, Galazka Z, Pietsch M, Uecker R, Fornari R (2011) Electrical properties of β-Ga_2O_3 single crystals grown by the Czochralski method. J Appl. Phys 110(6):063720
22. Oishi T, Koga Y, Harada K, Kasu M (2015) High-mobility β-Ga_2O_3 single crystals grown by edge-defined film-fed growth method and their Schottky barrier diodes with Ni contact. Appl. Phys. Express 8(3):031101
23. Zhang Z, Farzana E, Arehart A, Ringel S (2016) Deep level defects throughout the bandgap of (010) β-Ga_2O_3 detected by optically and thermally stimulated defect spectroscopy. Appl. Phys. Lett 108(5):052105
24. Jayawardena A, Ahyi AC, Dhar S (2016) Analysis of temperature dependent forward characteristics of Ni/β-Ga_2O_3 Schottky diodes. Semicond. Sci. Tech 31(11):115002
25. Fehse K, Walzer K, Leo K, Lovenich W, Elschner A (2007) Highly conductive polymer anodes as replacements for inorganic materials in high-efficiency organic light-emitting diodes. Adv. Mater 19:441–444
26. Sharma BK, Khare N, Ahmad S (2009) A ZnO/PEDOT:PSS based inorganic/organic heterojunction. Solid State communications 149:771–774
27. Matsuki N, Irokawa Y, Nakano Y, Sumiya M (2011) π-conjugated polymer/GaN Schottky solar cells. Sol. Energy Mater. Sol. Cells 95(1):284–287
28. Lozach M, Nakano Y, Sang L, Sakoda K, Sumiya M (2013) Fabrication of transparent conducting polymer/GaN Schottky junction for deep level defect evaluation under light irradiation. Phys. Status Solidi A 210(3):470–473
29. Kim MS, Jin SM, Choi HY, Kim GS, Yim KG, Kim S, Nam G, Yoon HS, Kim Y, Lee DY, Kim JS, Kim JS, Leem JY (2011) Fabrication and characterization of GaN/polymer composite p-n junction with PEDOT nanoparticle interface layer. Acta Physica Polonica A 119:875–879
30. Zhang D, Zheng W, Lin RC, Li YQ, Huang F (2019) Ultrahigh EQE(15%) solar-blind UV photovoltaic detector with organic-inorganic heterojunction via dual built-in fields enhanced photogenerated carrier separation efficiency mechanism. Adv. Func. Mater 29:1900935
31. Ewing D, Porter L, Wahab Q, Ma X, Sudharshan T, Tumakha S, Gao M, Brillson L (2007) Inhomogeneities in Ni/4H-SiC Schottky barriers: Localized Fermi-level pinning by defect states. J Appl. Phys 101(11):114514
32. Subramaniyam N, Sopanen M, Lipsanen H, Hong CH, Suh EK (2011) Inhomogeneous barrier height analysis of (Ni/Au)–InAlGaN/GaN Schottky barrier diode. Jpn. J Appl. Phys 50:030201
33. Shin, J. Park, S. Jang, T. and K. Sang Kim (2013) Metal induced inhomogeneous Schottky barrier height in AlGaN/GaN Schottky diode.Appl. Phys. Lett 102 (24) :243505.
34. Tekeli Z, Altndal S, Cakmak M, Özcelik S, Caliskan D, Özbay E (2007) The behavior of the I-V-T characteristics of inhomogeneous (NiAu)-Al0.3Ga0.7NAlNGaN heterostructures at high temperatures. J.Appl.Phys 102:054510
35. Oh S, Mastro MA, Tadjer MJ, Kim J (2017) Solar-blind metal-semiconductor-metal photodetectors based on an exfoliated β-Ga_2O_3 micro-flake. ECS J. Solid State. Sc. And Tech 6(8):79–83
36. Sasaki K, Higashiwaki M, Kuramata A, Masui T, Yamakoshi S (2013) Ga2O3 Schottky barrier diodes fabricated by using single-crystal Ga2O3 (010) substrates. IEEE Electr. Device Lett. 34:493–495
37. He H, Orlando R, Blanco MA, Pandey R, Amzallag E, Baraille I, Rérat M (2006) First-principles study of the structural, electronic, and optical properties of Ga2O3 in its monoclinic and hexagonal phases. Phys. Rev. B 74:195123
38. S. Li, Z. Y. Yan, Z. Liu, J. Chen,Y. S. Zhi, D. Y. Guo, P. G. Li, Z. P. Wu and W. H. Tang (2020) A self-powered solar-blind photodetector with large Voc enhancing performance based on the PEDOT:PSS/Ga2O3 organic-inorganic hybrid heterojunction (accepted).
39. Wang Z, Qi J, Yan X, Zhang Q, Wang Q, Lu S, Lin P, Liao Q, Zhang Z, Zhang Y (2013) A self-powered strain senor based on a ZnO/PEDOT:PSS hybrid structure. RSC Adv 3(38):17011
40. Zhang T, Wang F, Zhang P, Wang YF, Chen H, Li J, Wu J, Chen L, Chen ZD, Li SB (2019) Low-temperature processed inorganic perovskites for flexible detectors with a broadband photoresponse. Nanoscale 11(6):2871–2877
41. Zhang T, Wu J, Zhang P, Ahmad W, Wang YF, Alqahtani M, Chen H, Gao CM, Chen ZD, Wang ZM, Li SB (2018) High speed and stable solution – processed triple cation perovskite photodetectors. Advanced Optical Materials 6(13):1701341
42. Liu XZ, Guo P, Sheng T, Qian LX, Zhang WL, Li YR (2016) β-Ga_2O_3 thin films on sapphire pre-seeded by homo-self-templated buffer layer for solar blind UV photodetector. Optical Materials 51:203–207
43. Pratiyushi AS, Krishnamoorthy S, Kumar S, Xia Z, Muralidharan R, Rajan S, Nath DN (2018) Demostration of zero bias responsivity in MBE grown β-Ga_2O_3 lateral deep-UV photodetector. Jpn. J.Appl. Phys 57:06030313

44. Feng W, Wang X, Zhang J, Wang L, Zhang W, Hu P, Cao W, Yang B (2014) Synthesis of two-dimensional β-Ga_2O_3 nanosheets for high-performance solar blind photodetectors. J. Mate. Chem 2(17):3254–3259
45. Hu GC, Shan CX, Zhang N, Jiang MM, Wang SP, Shen DZ (2015) High gain Ga_2O_3 solar-blind photodetectors realized via a carrier multiplication process. Optics Express. 23(10):13554–13561
46. Pratiyush AS, Xia Z, Kumar S, Zhang Y, Joishi C, Muralidharan R, Rajan S, Nath DN (2018) MBE-Grown β-Ga_2O_3-Based Schottky UV-C Photodetectors With Rectification Ratio ~10^7. IEEE Photonics Technol. Lett 30:2025
47. Chen YC, Lu YJ, Lin CN, Tian YZ, Gao CJ, Dong L, Shan CX (2018) Self-powered diamond/β-Ga_2O_3 photodetectors for solar-blind imaging. J. Mater. Chem 6(21):5727
48. Wu Z, Jiao L, Wang X, Guo D, Li W, Li L, Huang F, Tang W (2017) A self-powered deep-ultraviolet photodetector based on an epitaxial Ga_2O_3/Ga:ZnO heterojunction. J. Mater. Chem 5(34):8688
49. Bai Z, Liu J, Liu F, Zhang Y (2017) Enhanced photoresponse performance of self-powered UV–visible photodetectors based on ZnO/Cu_2O/electrolyte heterojunctions via graphene incorporation. J. Alloys Compd 726:803

Publisher's Note

Springer Nature remains neutral with regard to jurisdictional claims in published maps and institutional affiliations.

Submit your manuscript to a SpringerOpen journal and benefit from:

- ► Convenient online submission
- ► Rigorous peer review
- ► Open access: articles freely available online
- ► High visibility within the field
- ► Retaining the copyright to your article

Submit your next manuscript at ► springeropen.com